Plasma Membrane Surface Increases with Tonic Stretch of Alveolar Epithelial Cells

Jacob L. Fisher, Irena Levitan, and Susan S. Margulies

Department of Bioengineering, Department of Pathology, and Institute for Medicine and Engineering, University of Pennsylvania, Philadelphia, Pennsylvania

Cyclic stretch stimulates numerous responses in alveolar epithelial cells—some beneficial, some injurious—often through mechanosensitive membrane-associated proteins such as stretch-activated ion channels. Tonic stretch, in contrast, stimulates only some of these responses. In this study, we hypothesized that the plasma membranes of alveolar epithelial cells expand during tonic stretch, not only through cell surface unfolding, but also through recruitment of additional phospholipids. Such plasma membrane expansion would reduce membrane tension and decrease stimulation of mechanosensitive membrane proteins. Primary rat alveolar epithelial cells were isolated, cultured for 48 h, and stretched between 3 and 40% change in basal membrane surface area. Gross changes in total cell surface area were obtained from stacks of thin fluorescent confocal micrographs; fine changes in plasma membrane area were measured via whole cell capacitance. A 1:1 correspondence linked changes in basal and total cell surface area, implying that cell surface area change is dominated by stretch of the attached basal surface. We also found that plasma membrane increased proportionally with surface area within 5 min of tonic stretch, showing that, given time to occur, plasma membrane expansion via lipid recruitment preponderates the changes in cell surface shape and size demanded by stretching the cell. Similarly, in cells tonically stretched 10 min to allow lipid insertion and then returned to an unstretched state, reabsorption of excess lipid occurred within 5 min. Finally, we found that lipid insertion induced by tonic stretch was unaffected by F-actin disassembly, ATP depletion, and calcium deprivation.

Stimulated by cyclic stretch, alveolar epithelial cells remodel their actin cytoskeletons (1), release cytokines (2), traffick ion-pumping proteins to the cell surface (3), secrete surfactant (4), accelerate type 2 to type 1 differentiation (5), modulate their gene expression, induce PKC activation and DNA synthesis (6), and decrease occludin and tight junction protein (7). Although the intracellular signaling pathways associated with these responses have been explored at length, they are diverse and complex, and generally remain to be fully elucidated (8). Equally unclear is how cells initially perceive the mechanical strain that triggers these signaling cascades. Nevertheless, two obvious hypotheses are widely considered: (*i*) mechanical stimuli open stretch-activated ion channels (SACs) in the plasma membrane, triggering intracellular signal cascades; and/or (*ii*) mechanical signals are transduced directly through focal adhesions and the cytoskeleton, stimulating intracellular processes.

(*Received in original form June 16, 2003 and in revised form March 10, 2004*)

Address correspondence to: Susan S. Margulies, Ph.D., Department of Bioengineering, University of Pennsylvania, 3320 Smith Walk, Philadelphia, PA 19104-6392. E-mail: margulie@seas.upenn.edu

Abbreviations: change in basement membrane surface area, ΔBSA; change in gross cell surface area, not including membrane folds, ΔCSA; cell surface area, coarsely measured, not including membrane folds, CSA; mechanosensitive membrane-associated protein, MMAP; stretch-activated channel, SAC; ventilator-induced lung injury, VILI.

Am. J. Respir. Cell Mol. Biol. Vol. 31, pp. 200–208, 2004
Originally Published in Press as DOI: 10.1165/rcmb.2003-0224OC on March 11, 2004
Internet address: www.atsjournals.org

Given currently available tools and technology for probing mechanically stimulated cells, SAC-associated signaling has been studied more often in alveolar epithelial cells, a trend continued in this communication. By blocking SACs with toxins such as gadolinium, investigators have inhibited calcium and sodium influxes known to trigger numerous stretch-associated signaling pathways in alveolar epithelial cells (8, 9). Studies have also shown that whereas some stretch-induced functions such as surfactant release respond to either cyclic (4) or static stretch (10), other effects, such as stretch-induced cell death (11) or stretch-induced Na^+/K^+-ATPase trafficking (3), are much less responsive to tonic or do not respond to tonic stretch at all. These findings indicate that some stretch-induced responses are not transduced as potently during tonic stretch as in cyclic stretch. Perhaps membrane tension arising from cyclic deformations rises and falls too quickly for the plasma membrane to remodel. Although we do not test this possibility directly in this study, we test an alternative hypothesis that, with tonic stretch, the plasma membrane gradually expands by insertion of additional phospholipid membrane from an intracellular reservoir, reducing membrane tension below the threshold for stimulating particular membrane-dependent stretch-induced responses.

Plasma membrane vesiculation (to restore tension) and vesicle recruitment (to relieve tension) are already known to occur in a variety of cell types and artificial bilayer vesicles. In artificial liposomes, a flaccid bilayer will bud and vesiculate until it becomes a sphere, minimizing surface area, the liquid/liquid interface, and hence free energy (12). Red blood cells also become flaccid, vesiculate, and fragment after cytoskeletal disruption (13). On the other hand, high membrane tension favors fusion of shed vesicles with the parent membrane to lower the total energy of the system (13). Confirming this theory, Raucher and Sheetz identified a plasma membrane reservoir in chick embryo fibroblasts (14). When membrane tethers were pulled, plots of tension versus tether elongation reveal what the investigators labeled an initial phase, an elongation phase, and an exponential phase. In another study, Dai and coworkers found that membrane tension and cell surface area interact in a tightly regulated feedback loop (15). In some cell types membrane remodeling is rapid, and one can see vesicles merging with or being absorbed from the plasma membrane with simple light microscopy (15). In other studies lipid trafficking is slower and subtler, and has been tracked by measuring total cell capacitance or visualized with lipid dyes, such as FM 1–43 (16–20) or various sphingolipids (21–23), and captured using confocal fluorescent microscopy.

In many of the studies cited above, total cell capacitance was the preferred method of tracking changes in plasma membrane area. In essence the lipid bilayer of the cell membrane is an insulator that can bear a capacitive charge on its surface directly proportional to its surface area. Thus, by piercing a cell with a micropipette and measuring capacitance between the cytosol and the extracellular milieu, one can assess the surface area of the plasma membrane and changes in it with great sensitivity (24, 25). Frequently this technique has been used to observe endo- and exocytosis rates in secretory cells, as vesicles merge

with and retract from the plasma membrane (26–29), because it is sensitive to small changes in cell surface area. Further, because electrical charge distributes throughout even the smallest spaces, capacitance is an excellent means of measuring surface area regardless of the shape of the cell and cell membrane ruffling. This independence of whole cell capacitance from the ruffling or smoothness of the cell membrane is especially important in determining the membrane size of animal cells, which generally possess a stable excess of membrane area used precisely for buffering rapid deformation and tension changes (13). Other cells respond to deformation in two phases with initial plasma membrane unfolding, followed by vesicular recruitment (13, 30). Studies of bladder epithelial cells, for example, found that the apical cell surface unfolds during initial bladder filling, but accommodates further volume changes during the latter phase of filling by insertion of cytoplasmic vesicles (30). In each of these studies, measurement of total cell capacitance served as an invaluable means of distinguishing between cell surface expansion via unfolding and expansion via lipid insertion. With this technique, a cell that swells or changes shape by membrane unfolding will not change its capacitance, but its apparent area will increase in light micrographs. On the other hand, if lipid bilayer is added to the cell membrane during events like cell stretch or exocytosis, capacitance, as well as apparent surface area, will increase.

Alveolar epithelial cells can potentially expand via either mechanism. On one hand, electron photomicrographs show that alveolar epithelial cells possess a ruffled membrane (20). Furthermore, under normal physiologic function these cells are repeatedly stretched and released at a rate greater than known lipid recruitment could take place, yet they do not rupture, indicating that the deformation has likely been accommodated by the more rapid mechanism of membrane unfolding. On the other hand, Vlahakis and colleagues, using lipid staining methods, found that lipid trafficking occurred in statically deformed alveolar type 2 cells (20). However, using these methods, increases in plasma membrane surface area cannot be assessed, for the measured increase in lipid insertion may be accompanied by increased lipid recycling. Indeed, tonically stretched alveolar type 2 cells have been reported to increase rates of both exocytosis (20) and endocytosis (31). But to remodel the cell surface in a way that relieves membrane tension, exocytosis must outpace endocytosis and the plasma membrane must undergo a net expansion.

In this study we have hypothesized that the increase in alveolar epithelial cell lipid insertion observed during static stretch results in net plasma membrane expansion, and we set out to quantify this expansion. We rationalized that given the broad, flat shape of alveolar epithelial cells, the cell surface area must increase during imposed alveolar epithelial stretch to accommodate a 25% increase in basal surface of area. We assume that this increase in cell surface area likely occurs through a combination of fast membrane unfolding and slower lipid insertion. The studies presented here quantify changes in cell size, cell surface area, and plasma membrane area to distinguish between plasma membrane growth and unfolding during tonic stretch. This is done by imaging stretched and unstretched cells using fluorescent laser confocal microscopy, calculating changes in cell volume and surface area, and measuring change in capacitance over the plasma membranes of stretched and unstretched alveolar epithelial cells. Additionally, we explore potential pathways and dependencies of stretch-induced plasma membrane expansion by depleting cellular ATP, disrupting the actin cytoskeleton with latrunculin, eliminating extracellular calcium and sequestering intracellular calcium. These broad spectrum disruptions were chosen because ATP reserves, a dynamic, functional cytoskeleton, and calcium transients have been shown to play critical roles in other cellular insertion pathways.

Some of the results of these studies have been previously reported in the form of an abstract (32).

Materials and Methods

Cell Isolation

Alveolar type 2 cells were isolated from male, Sprague-Dawley rats (Charles River, Wilmington, MA) according to a previously described protocol (11) approved by the University of Pennsylvania IACUC. Briefly, animals were anesthetized with sodium pentobarbital (50 mg/kg, injected intraperitoneally). The trachea was cannulated, the lungs mechanically ventilated, and the animal exsanguinated per abdominal aortotomy. The heart was pierced and the lungs were perfused via the pulmonary artery. The lungs were subsequently excised and type 2 cells were isolated using an elastase digestion adapted from Dobbs and coworkers (33), in which the lungs are instilled and incubated with an elastase solution (3 U/ml; Worthington Biochemical, Lakewood, NJ) and then minced with a tissue sectioner (Sorvall, Newtown, CT). Cells were filtered through a series of sterile progressively finer Nitex mesh (Crosswire Cloth, Bellmawr, NJ), and plated on a suspension culture dish coated with rat IgG (3 mg IgG per 5 ml Tris-HCl incubated overnight and rinsed; Sigma, St. Louis, MO). After a 1-h incubation at 37°C, gentle panning lifted type 2 cells from macrophages and other contaminating cells preferentially adhered to the culture dish. Finally, cells were spun down and resuspended in MEM supplemented with Earle's salts, 10% fetal calf serum, and 25 μg/ml gentamicin (Life Technologies, Rockville, MD).

Cell Culture

Alveolar type 2 cells were seeded at a density of 1×10^5 cells/cm^2 on fibronectin-coated (42 μg/ml; Boehringer Mannheim Biochemicals, Indianapolis, IN), flexible Silastic membranes (Specialty Manufacturing, Saginaw, MI) mounted in custom-made wells, which could be used for cell stretching on a microscope stage. This created a nonconfluent culture so that whole cell capacitance could be measured in individual cells without the concern of conductive cell-cell connections artificially inflating capacitance values. Cultures were maintained for 48 h at 37°C under 5% CO_2 in MEM supplemented with Earle's salts, 10% fetal bovine serum, and 25 μg/ml gentamicin (Life Technologies).

Laser Confocal Microscopy and Image Analysis

Before imaging, cells were loaded with calcein AM, a fluorescent cytosolic dye (30 min, 37°C, 5% CO_2) in Dulbecco's modified Eagle's medium without $NaHCO_3$, supplemented with 1% penicillin (1,000 U/ml)/streptomycin (10 mg/ml) (Life Technologies) and 20 mM HEPES (Sigma). Wells ($n = 3$) were then mounted in a custom-made stretching device, and image slices were captured through the depth of 3–5 randomly selected unstretched cells in the field of view (per well) using a z-step of 0.25–0.3 μm on a Nikon TE300/Bio-Rad Radiance 2,000 laser confocal fluorescent microscope, a Nikon 40×/0.75 Plan-Fluor objective and Bio-Rad LaserSharp software (Nikon Corporation, Melville, NY; Bio-Rad Laboratories, Hercules, CA). Wells were then stretched to 25%ΔSA by means of a computer-controlled stepper motor pushing an annular indenter against the Silastic membrane, on the side opposite the attached cells. The same cells previously imaged in the unstretched state were relocated and imaged again in the stretched position. Using Scion Image (Scion Corporation, Frederick, MD) slice images were median filtered to reduce background noise and to smooth noisy cell boundaries. Cells were then traced and their cross-sectional area and perimeter were measured using the Scion Image Particle Analysis function. From each image stack, cell volume was calculated by numerical integration (Simpson's Rule [34]) of cell cross-sectional areas over cell height. Total cell surface area (CSA) was calculated by numerically integrating conic section surface areas from each image slice over cell height. From paired image stacks of the same cell stretched and unstretched, a relationship was determined between the change in basal surface area (ΔBSA), determined from the area change of the largest, most basal image slice, and the change in total cell surface area (ΔCSA) calculated here.

Capacitance Measurements and Comparisons

Previous studies have demonstrated that cell capacitance scales linearly with plasma membrane area (25, 35). Using this relationship, investigators have tracked mechanically induced lipid insertion via whole-cell capacitance measures in a variety of cell types (15, 25, 36–38). Some investigators have used high resolution patch-clamp capacitance recording in the femto- and attofarad range to detect individual exocytotic events (39, 40) and even to discriminate among different sized exocytotic vesicles according to capacitance step magnitude (41). Together with confocal microscopy studies of cells before and after stretch, cell capacitance data let us distinguish between cell surface expansion via plasma membrane unfolding or net plasma membrane accumulation via lipid insertion.

In preparation for experiments in room air, MEM was aspirated from cells and replaced with Dulbecco's modified Eagle's medium without $NaHCO_3$, supplemented with 1% penicillin (1,000 U/ml)/streptomycin (10 mg/ml) (Life Technologies) and 20 mM HEPES (Sigma). All cells were kept at 37°C until the moment wells were mounted on the microscope stage for measuring capacitance. Unstretched control wells were mounted in the stretching device but not stretched. Wells in the experimental stretch group were mounted in the stretch device and stretched immediately by screwing the well down against an annular indenter that pressed on the Silastic membrane on the side opposite the attached cells, causing equibiaxial stretch of the Silastic membrane ($\sim$ 25% change in surface area) and the adherent cells (11).

Glass micropipettes were pulled to a resistance of 4–6 MΩ, loaded with a solution of (in mM): 156 KCl, 1.5 $CeCl_2$, 1 $MgCl_2$, 10 HEPES, 1 EGTA, pH 7.3, and mounted over a silver electrode. A saturated salt agar bridge placed in the extracellular medium served as a reference electrode. Electrophysiologic measurements were made with an EPC9 amplifier and its companion Pulse software (HEKA Electronik, Lambrecht, Germany). Using a micromanipulator, the micropipette was brought into contact with the cell membrane, and a seal was formed using a small, manually applied negative pressure in the micropipette. Electrode potential was set at −60 mV and pipette capacitance was compensated automatically in the Pulse software before perforating the cell membrane by manually applying quick negative pressure pulses through the patch electrode. Under optimal conditions a successful patch could be made and perforated, and whole cell capacitance and series resistance could be measured in 5 min. Thus, in stretched wells, the earliest measurements were made 5 min after the stretch event. (In unstretched wells, this lag was not as relevant, as there was no stretch event.) Generally multiple cells were probed in each well, though no well was kept on the microscope at room temperature for more than 40 min. Thus all measurements were made within 5–40 min of mounting the well on the microscope, which coincided with the moment of stretch for stretched wells. On average, one to six cells were successfully probed in each of six to eight wells for each experimental group (three to four stretched wells and three to four unstretched control wells). Exact numbers of samples are given in the results of individual experiments.

In another set of experiments, seven cells were stretched tonically for 10 min and then returned to an unstretched state before capacitance was measured. Again, creating a perforated patch clamp required $\sim$ 5 min so that the earliest measurements were made 5 min after the cell was "unstretched." In three of the seven cells, capacitance was recorded for 5 min (i.e., the period from 5 min post-stretch to 10 min post-stretch) to determine whether capacitance was still decreasing or if a steady state had been reached. In the remaining four cells, the patch-clamp did not last for an entire 5-min recording period.

After a cell was probed, a photomicrograph was captured using a Nikon camera and Kodak ISO 100 print film. Micrographs were digitally scanned and stored as TIFF arrays. Using Adobe Photoshop, cell boundaries were traced with the magnetic lasso tool, and contrast was enhanced between cells and background. Basal surface area was measured in each contrast-enhanced image using the Scion Image Particple Analysis tool and then used to plot cell capacitance as a function of projected cell surface area for stretched and unstretched cell groups.

Treating Cells

Previous studies have shown that vesicular trafficking in alveolar epithelial cells is sometimes dependent upon normal functionality and integrity of the actin cytoskeleton (42) and is often stimulated by increased intracellular calcium, brought about by calcium influx into the cell or intracellular calcium release (43). In other cell types, lipid insertion and insertion into the plasma membrane has been shown to be ATP-dependent (44, 45). In urothelial cells, which expand via initial plasma membrane unfolding and subsequent vesicular insertion during bladder filling, translocation of vesicles into and out of the apical membrane was dependent on intact microfilaments but not an intact microtubule system (46). ATP was also required for vesicle insertion during stretch but not vesicle endocytosis during bladder collapse (47).

To test the dependence of tonic stretch-induced lipid insertion on integrity of the actin cytoskeleton, additional capacitance experiments were performed with cells that were pretreated for 1 h with latrunculin A (100 nM; Sigma), which sequesters G-actin to prevent dynamic F-actin remodeling. In other cells, ATP levels were depleted for 1 h before study using the glycolytic metabolic inhibitors 2-deoxy-D-glucose (2 mM; Sigma) and antimycin A (10 μM; Sigma), which have been shown to reduce intracellular ATP levels 45–90% in cultured epithelial cells (48). Finally the effects of Ca^{2+} were tested first by stretching cells in a Ca^{2+}-free medium to isolate the effect of Ca^{2+} influx and next by using Ca^{2+}-free medium after also sequestering intracellular Ca^{2+} for 1 h using BAPTA-AM (50 μM; Molecular Probes, Eugene, OR). Capacitance was measured in 4–12 stretched and 4–12 unstretched cells in each treatment group (exact numbers for each group given in results). Images were captured and processed as described above for stretched, untreated cells.

Data Analysis

In studies comparing changes in projected cell surface area to total cell surface area, all data were captured from paired image stacks of the same cells before and after stretch. The image slice that contained the greatest cellular cross-sectional surface area was designated the basal slice, and the cross-sectional area of the cell or cells in this slice was defined as basal surface area. Also in the basal slice, where cell boundaries were most crisp, we selected a lower bound intensity threshold to eliminate background signal, using the guide that it be as high as possible without cropping any part of the cell image. This threshold parameter was used in the Scion Image Particle Analysis tool for all slices within a cell. Cell volume was calculated using Simpson's Rule (34) to calculate the area under the curve of slice area versus slice height. Total cell surface area was calculated using Simpson's Rule to sum surface area sections of slice-by-slice conic sections.

To extract change in plasma membrane surface area from measured changes in capacitance, we used a parallel plate capacitor relationship between cell capacitance, C, and plasma membrane surface area, A: $C = \varepsilon A/d$, where ε is the dielectric modulus of the plasma membrane and d is membrane thickness. Energetic constraints limit change in membrane thickness to $d < 3.6\%$ (13), and the only possible change in dielectric modulus ε might be a small decrease resulting from rarefaction of the lipid bilayer, which would *decrease* measured capacitance. Thickness and dielectric modulus being relatively constant, observed increases in capacitance can be attributed primarily to increased plasma membrane surface area, as established by other investigators (25, 35).

Because micropipette probing to measure capacitance is a destructive technique, we are unable to probe the same cell twice to measure a change in capacitance with stretch. Hence, we must look for a change in the capacitance versus size relationship between stretched and unstretched cells (Figure 1). If a group of cells is stretched and their apparent surface areas increase by membrane unfolding *without lipid insertion* (and without the consequent increase in capacitance), the capacitance versus surface area regression line will shift to the right, but not upward. In this case, the capacitance-area regression line in the stretched cells would be distinct from that in unstretched cells. However, if the surface area of stretched cells increases *solely via lipid insertion* into the plasma membrane, the capacitance versus surface area relationship will shift both to the right and upward, as both surface area and capacitance increase. In this second limiting case, the capacitance-area regression line would coincide with the unstretched cells, as if the stretched cell had the same capacitance and plasma membrane surface area of a large unstretched cell, a state it can achieve after stretch only by lipid insertion.

The standard statistical approach for detecting differences in two regression lines is an analysis of covariance (ANCOVA). ANCOVA

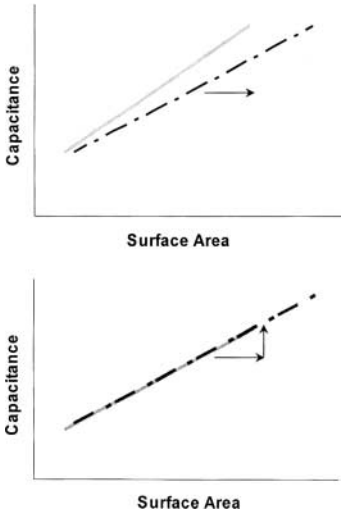

Figure 1. Capacitance and surface area in two membrane expansion models. If plasma membrane expansion occurs via membrane unfolding, the capacitance versus area relationship for a group of cells (*top panel, gray solid line*) will shift to the right as cells grow larger with stretch (*top panel, black dashed line*). However, if the plasma membrane does not unfold but expands by adding additional lipid, the line will shift both to the right with stretch and upward with increased capacitance (*bottom panel, black dashed line*). If the lines coincide, as shown here below, the relationship between surface area and capacitance is conserved, meaning a stretched cell has increased the size of its plasma membrane in proportion to its size and looks simply like a larger unstretched cell. The coincidence of the stretched and unstretched cell plots, fit to real data with a certain degree of variability, is tested by ANCOVA, which essentially measures the parallelism and distance between two regression lines.

is used for testing a hypothesized difference between two sets of values while factoring out the effect of a covariate. It is appropriate to use ANCOVA to test a difference in capacitance between stretched and unstretched cells while factoring out how capacitance varies with area (the covariate in this example). Because we hypothesize that tonic stretch stimulates lipid insertion rather than membrane unfolding, we expect ANCOVA to detect no difference between stretched and unstretched groups. A null hypothesis can be accepted only after a power analysis is performed to ensure that ANCOVA and the given data have sufficient statistical power to detect a difference if a true difference exists. To perform a power analysis, we simulated separation between the stretched and unstretched data sets by increasing the gap in capacitance, by increasing stretch without adjusting capacitance, or by increasing capacitance in stretched cells between a pure unfolding model and a pure lipid insertion model. We created power curves for each simulation. From these curves we determined the smallest change in capacitance, the smallest amount of stretch without capacitance, and the smallest amount of lipid insertion without unfolding that can be detected (at 80% power) given the collected data (W. J. Ewens, personal communication to J.L.F., Sept.–Oct. 2003), and thus constructed a confidence interval for concluding the null hypothesis.

Results

Nonconfluent Cells Stretch Similarly to Confluent Cells

Confocal microscopy experiments in this study observed a cellular ΔBSA of 25.0% ± 10.6% (mean ± SD) in nonconfluent cells with a 25% ΔSA stretch of the substratum Silastic membrane. These results were statistically indistinguishable in both mean ($P > 0.5$) and variance ($P > 0.05$) from results of previous studies that found that confluent epithelial monolayers on a Silastic membrane stretched to 25% ΔSA changed by ≈ 24% ± ≈ 7% (mean ± SD) (11). We did note, however, that larger cells with greater basal surface area in contact with the underlying membrane stretched closer to 25% ΔBSA with less variability than smaller cells.

This study was performed on nonconfluent cells to avoid artifacts in measurement of cell capacitance that are due to electrical coupling between cells. To maintain consistent conditions throughout all experiments and to allow for result comparison, nonconfluent cells were used in all experiments. Analyses of the studies were paired so that differences between Silastic membrane and actual cell stretch magnitudes did not affect ultimate results. In confocal microscopy studies correlating ΔBSA to ΔCSA, each stretched cell was compared with its own unstretched image. In capacitance studies, capacitance was recorded in stretched and unstretched cells as a function of the absolute value of basal surface area, not ΔBSA. Thus, as long as stretched cells received a different stimulus from unstretched cells—and they did stretch on average 25.0% ΔBSA—variation around the 25% ΔSA of the Silastic membrane is not an important detraction.

Increases in Overall Cell Surface Are Strongly Linked to Changes in Basal Surface Area

In stretched cells we detected a very close correlation between percent ΔBSA and the percent ΔCSA (Figure 2). Volume changes, however, were more variable; some of the tested cells ($n = 5$) increased their volume in proportion to basal stretch, whereas other cells flattened ($n = 4$) during stretch, leading to only small increases and, in some cells, even slight decreases in volume (Figure 3). A geometric analogy, which helps to explain the close match between ΔCSA with ΔBSA and also the mismatch between ΔBSA and volume, considers alveolar epithelial cell shape to be similar to a short cone with a broad base. The surface area of a cone is the area of the base, $A = \pi r^2$, plus the lateral surface, $S = \pi r (r^2 + h^2)^{1/2}$. Volume, V, is equal to Ah/3, where r is the radius of the base and h is the height of the cone. For a very short, very wide cone ($r >> h$), a change in total surface area (that is, ΔCSA in the cells in this study) is nearly proportional to a change in the area of its base (ΔBSA), but is affected little by change in height (Δh). In contrast, volume is equally dependent on both basal area and height. This general concept holds for any geometric solid with a base dimension much greater than its height. Cells in this study generally had dimensions of r ≈ 50–60 μm and h ≈ 3–4 μm. Hence with alveolar epithelial stretch, ΔCSA was predominantly dependent on imposed ΔBSA, whereas volume changes were equally dependent on variable changes in cell height or thickness with stretch and reflect that same randomness. Because the cell did not maintain constant proportions with stretch, it did not fulfill a two-thirds power rule between ΔBSA (or ΔCSA) and ΔV. In fact, all volume increases were less than the two-thirds power rule predictions.

Plasma Membrane Enlarges with Stretch

In cells stretched and held for 5 min or more ($n = 14$), the linear relationship between capacitance and area remained statistically indistinguishable from that of unstretched cells ($n = 14$) (Figure 4). Power analysis showed that for the given data and standard criteria of 80% power and $P < 0.05$ to determine significance, any increase in cell size > 7.27% ΔBSA without a change in capacitance would generate a statistically detectable and significant difference

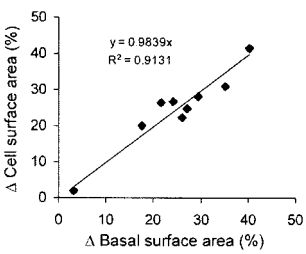

Figure 2. Change in total cell surface area versus change in basal surface area. In stretched cells, the percent ΔCSA was highly correlated with percent ΔBSA. This is due primarily to the broad flat geometry of the cultured alveolar epithelial cell. This is consistent for a geometric solid with a base dimension much greater than its height, where changes in total surface area are closely correlated with changes in the area of the broad base.

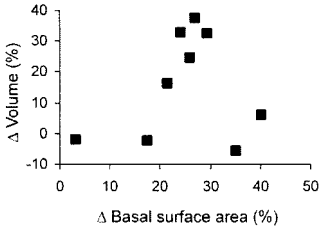

Figure 3. Change in cell volume versus change in basal surface area. Stretch-induced change in cell volume did not correlate with ΔBSA, primarily due to a lack of correlation between stretch and change in cell height. Unlike overall CSA, which varied directly with the basal area (Figure 2) but remained virtually independent of fluctuating cell height, cell volume depended upon both basal area and height changes. Some cells flattened with stretch, but others did not, and this randomness in height changes is reflected in volume changes.

between regression lines. Because cells were stretched to a 25% ΔBSA increase and no difference was detected, we conclude that stretched cells enlarged their area and also increased in capacitance, which is possible only with plasma membrane expansion. Our power analysis demonstrated that the detectable limit was 74.6% lipid insertion; any combination with less insertion and more unfolding than 74.6% insertion/25.4% unfolding would be detectable. Hence, although we cannot rule out the possibility that up to 25.4% of the imposed ΔCSA might be due to unfolding, lipid insertion accounts for the clear majority of ΔCSA after 5 min of tonic stretch. Because capacitance could not be measured any sooner after stretch than 5 min, this finding does not reflect the relative contributions of plasma membrane unfolding and lipid insertion immediately after stretch. Nonetheless these findings do support the concept of lipids inserting into the plasma membrane during prolonged tonic stretch.

Enlarged Plasma Membrane Contracts with 5 min of Unloading

The relationship between size and capacitance of stretched cells that were released was similar to that of control cells that had never been stretched. Recall that stretch increased the capacitance as well as size of the cells. Interestingly, upon release, both cell area and cell plasma membrane volume decreased, and none of the increased plasma membrane lipid inserted during tonic stretch had been retained (Figure 5). These measurements demonstrate that stretched cells that were returned to their initial size after a period of tonic stretch reabsorbed excess plasma membrane and achieved a steady, restored initial state within 5 min. Current technique prevented measuring dynamic capacitance change earlier than 5 min after release from stretch. Capacitance measured over a subsequent 5 min in three stretched and released cells did not change, indicating steady state had been achieved.

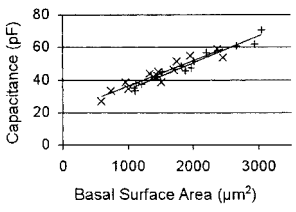

Figure 4. Capacitance versus basal surface area in stretched and unstretched cells. The relationship between basal surface area and whole cell capacitance did not change significantly between stretched (+) and unstretched (×) cells, as shown by the statistically indistinguishable slope and elevation of the regression lines. This persistent relationship indicates that the plasma membrane expands with stretch to account for increased cell surface. Hence, the plasma membrane area of a tonically stretched cell is no different from that of a larger unstretched cell. In contrast, if plasma membrane expansion did not occur and the cell surface increased through membrane unfolding, the stretched data would shift to the right as area increased without shifting upward in capacitance.

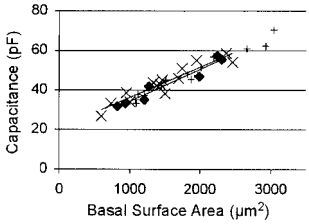

Figure 5. Capacitance versus basal surface area in stretched, unstretched and stretched and released cells. Compared with stretched (+) and unstretched (×) cells the relationship between capacitance and surface area did not change in cells that had been stretched for 10 min and then unstretched (*diamonds*). As shown at left, cells that were stretched for 10 min to allow lipid insertion and then returned to their original size (*diamonds*) also returned to a lower capacitance within 5 min, reabsorbing membrane rather than keeping the enlarged tonic stretch capacitance.

Lipid Insertion Independent of Ca^{2+}, ATP Resources, and Cytoskeleton Integrity

Although calcium fluxes, ATP-based energy resources, and an intact cytoskeleton have been proved necessary for some cellular insertion functions, perturbing them had no effect on stretch-induced insertion. In cells treated with latrunculin A ($n = 8$, stretched; $n = 4$, unstretched) and cells depleted of ATP ($n = 9$, stretched; $n = 5$, unstretched), the regression lines of stretched and unstretched cells remained statistically indistinguishable (Figures 6 and 7). As concluded in untreated cells, this consistent relationship between cell capacitance and cell surface area between stretched and unstretched cells demonstrated that stretched cells with larger basal surface areas had undergone proportional plasma membrane growth via lipid insertion, rather than surface unfolding. Furthermore, neither eliminating extracellular calcium ($n = 12$, stretched; $n = 4$, unstretched) nor sequestering intracellular calcium and eliminating extracellular calcium together ($n = 6$, stretched; $n = 8$, unstretched) had any effect on cell capacitance before stretch or tonic stretch-induced lipid insertion and plasma membrane expansion (Figures 8A and 8B).

It was interesting to note, however, that after 1 h of G-actin sequestration or ATP depletion, capacitances had increased significantly ($P < 0.05$ by ANCOVA) in treated cells relative to untreated cells, whether examining the stretched or unstretched condition.

Thus, whereas these two treatments promoted plasma membrane expansion *before* cells were stretched, they did not preclude further lipid insertion and plasma membrane growth with tonic stretch.

Discussion

Alveolar epithelial cells are resilient to stretch by necessity. Attached to the inside surface of repeatedly inflating and deflating alveoli, these broad, flat cells need to withstand repeated deformations, which are generally small in a person breathing at rest but can reach a 37% ΔBSA during deep inspiratory

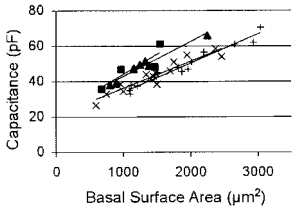

Figure 6. Capacitance versus basal surface area after latrunculin treatment. In cells treated with latrunculin to disrupt the actin cytoskeleton, the plasma membrane expanded even in unstretched cells (*squares*), as shown by increased capacitance. When latrunculin-treated cells were stretched tonically (*triangles*), capacitance increased further, indicating that stretch-induced lipid insertion and plasma membrane expansion do not depend upon the integrity of the actin cytoskeleton. Stretched (+) and unstretched (×) untreated controls (from Figure 4) are shown for comparison.

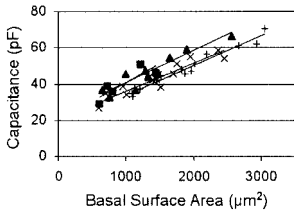

Figure 7. Capacitance versus basal surface area after ATP depletion. Like latrunculin treatment, ATP depletion brought about plasma membrane expansion even before cells were stretched, but the treatment had no effect on additional, tonic stretch-induced membrane expansion. Because ATP is required for actin polymerization, ATP depletion could be causing the same effect as latrunculin treatment. This finding also indicates that plasma membrane expansion does not depend on ATP as an energy source for lipid insertion. Shown are stretched (*triangles*) and unstretched (*squares*) ATP-depleted cells, and stretched (+) and unstretched (×) untreated control cells from Figure 4.

maneuvers. Mechanical ventilation in diseased or injured lungs with inhomogeneous parenchymal mechanical properties and surfactant dysfunction can lead to uneven distribution of inspired gas with unusually high regional inflation and even greater, supraphysiologic epithelial strain (49). Frequently, such overinflation can trigger what is aptly dubbed ventilator-induced lung injury (VILI), a syndrome whose symptoms can include pneumothorax, alveolar edema, changes in pulmonary mechanics and lung cell function and, ultimately, lung cell death (49). VILI is especially concerning in patients already suffering from acute respiratory distress syndrome (ARDS), where VILI has an incidence of 5–15% and an associated mortality of 34–60% (50). But even in normal lungs, VILI can occur with high tidal volume mechanical ventilation (49). Therefore, how alveolar epithelial cells and their plasma membranes routinely accommodate physiologic strains and the consequences of exceeding strain tolerances are particularly germane to understanding VILI.

Recently, Vlahakis and Hubmayr proposed four possible ways in which plasma membrane could respond to stretch: (*i*) stress failure, (*ii*) insertion of additional lipids from intracellular stores to the plasma membrane, (*iii*) increased intramolecular distance in the lipid bilayer, or (*iv*) plasma membrane unfolding (51). They have identified the first two mechanisms in their own studies under particular stretch conditions; stress failure appeared when A549 alveolar epithelial cells were stretched at high strain rates (52), and lipid insertion took place in tonically stretched A549 cells (20). Energy considerations of phospholipid hydrophobicity rule out increasing molecular distances as a significant factor. Biological membranes can only sustain elastic expansion of $< 3\%$ before failure. The fourth proposal, plasma membrane unfolding, remains a likely means of accommodating membrane stretch at medium strain rates, which are not so explosive as to cause stress failure, but are still faster than lipid insertion alone could accommodate. It is also possible that even after 5 min of tonic stretch, when we observed lipid insertion, membrane unfolding still could account for up to 25% of the total cell surface increase and remain statistically undetectable in our data. By measuring changes in membrane capacitance, the present study not only used a new technique to confirm that lipid insertion occurs during tonic stretch of alveolar epithelial cells in primary cultures but also showed that stretch stimulates a net plasma membrane expansion sufficient to account for at least 75% of the entire increase in cell surface area. Because of the time required to take a capacitance reading after stretch, our findings cannot predict relative contributions of membrane unfolding and lipid insertion in the short term. In fact, because lipid insertion cannot occur as quickly as unfolding, unfolding is probably more important in buffering the immediate cell response to stretch. Nevertheless within 5 min of tonic stretch, membrane expansion via lipid insertion accounts for the majority of surface area changes, relieving plasma membrane stress and potentially allowing the cell surface to refold (Figure 9).

Under various physiologic conditions across cell types, plasma membrane expansion via lipid insertion appears to serve as a protective buffer against high membrane tension and potential stress failure. The ultimate strain capacity of biological membranes is $< 3\%$, or $< 6.1\%$ ΔSA under equibiaxial stretch. Hence the plasma membrane must be supplemented with additional phospholipids to avoid stress failure during any cell deformation beyond this limit. Neuron, muscle, and epithelial cells have all been shown to add membrane from intracellular stores when swollen by osmotic perturbation and to reabsorb membrane upon reshrinking. Laser tweezers can be used to pull a membrane tether from a cell and monitor relaxation and recovery of membrane tension during such events. With osmotic shrinking and swelling, membrane tension and surface area appeared to be linked in a feedback mechanism that tightly constrains the range of membrane tension. In similar studies, tethers pulled from fibroblasts recorded an initial increase in tension as the tether formed, but then tension remained constant as the tether was pulled further at a constant rate. Only at very high strains did tension begin to increase again (14). This plateau in which strain increased with no increase in tension is attributed to lipid insertion into the plasma membrane from a tension-buffering reservoir. In attached alveolar epithelial cells, stretching the basement membrane stimulated lipid insertion to the cell surface, detected

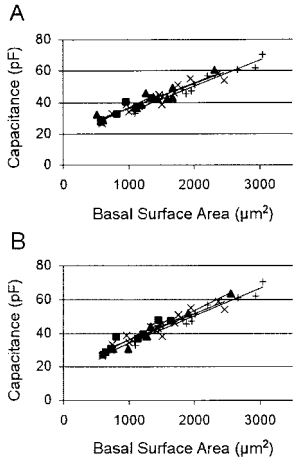

Figure 8. Capacitance versus basal surface area in calcium-depleted cells. Neither depleting calcium in the extracellular medium alone (*A*) nor depleting extracellular calcium and sequestering intracellular calcium (*B*) affected cell capacitance. Cell capacitance increased with cell size in tonically stretched cells regardless of calcium depletion, indicating that tonic stretch-induced lipid insertion occurs independent of calcium levels or signaling. Shown are stretched (*triangles*) and unstretched (*squares*) calcium-deprived cells, and, for comparison, stretched (+) and unstretched (×) untreated control cells (from Figure 4).

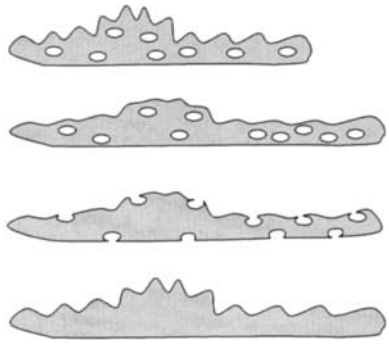

Figure 9. Lipids are inserted during tonic stretch and account for the greatest part of surface area increases. In summary, our results confirmed that tonic stretch results in lipid insertion and plasma membrane expansion. In this series of cartoons, the cell begins unstretched. Because apparent surface area increases faster than lipid insertion is known to occur, surface unfolding is presumed, though we have not demonstrated that in this study. Then, according to our results, additional lipid is added to the plasma membrane, increasing the cell surface area. Within 5 min the plasma membrane has expanded and refolded such that the membrane capacitance of a stretched cell appears little different from that of a large unstretched cell. This phenomenon persists even after actin derangement, intracellular ATP depletion, or calcium sequestration.

by dye dilution in the plasma membrane (20). Although this prior study did not discriminate between net lipid insertion and lipid recycling, which could possibly produce no net plasma membrane expansion, the results of the present study show that the plasma membrane does expand and that this expansion accounts for at least 75% of the total stretch-induced change in cell surface area.

Our finding that alveolar epithelial plasma membrane expansion takes place within 5 min of tonic stretch also sheds light on the reported discrepancy between functional sensitivity to cyclic and tonic stretch stimuli. Previously we found that Na^+-K^+-ATPase activity is stimulated by 1 h of cyclic stretch, and that this stimulus was significantly dependent upon SAC function (3). One hour of tonic stretch, in contrast, had no effect. The present study clarifies that tonically stretched plasma membrane expands via lipid insertion within the first 5 min of stretch. In cyclic stretch, the opening of SACs is made energetically favorable by cyclically repeating increases in membrane tension. But as lipids insert and the plasma membrane expands to relieve membrane tension, SAC opening would become energetically unfavorable. Stretch-induced cell death, and other cell functions that exhibit a similar contrast between cyclic and tonic stretch responses, may also be related to SACs or other MMAPs, which are no longer stimulated once lipid insertion occurs in tonic stretch. Meanwhile, cell functions such as surfactant secretion, which are stimulated by either cyclic or tonic stretch, are probably not signaled through plasma membrane tension and MMAP stimulation, but rather through other potential stretch transducers such as the cytoskeleton.

Unlike many cellular insertion mechanisms, our results demonstrate that stretch-induced lipid insertion is not dependent on calcium, ATP availability, or cytoskeletal integrity. Similar calcium-independent, tension-regulated lipid insertion is found in plant cells (53) and osmotically swollen neurons (37, 54). Morris and colleagues argue from cellular energy economy that a tension-regulated lipid insertion mechanism is not only experimentally evident but also theoretically appealing (35). Rather than depend upon dissipating ion gradients and complex signaling pathways, high membrane tensions could act as both signal and potential energy source for lipid insertion. This could also explain the null effect of ATP depletion on stretch-induced capacitance increases; if tension provides the necessary well of potential energy, insertion would not have to depend upon another cellular energy source, like ATP.

Although cytoskeleton disruption with latrunculin and ATP depletion did not affect plasma membrane expansion with stretch, they did bring about a capacitance increase even in unstretched cells. Disassembly of the cytoskeleton has previously been shown to increase cell capacitance (55–57) and decrease membrane tension (58, 59). Two mechanisms have been proposed for this. On one hand, breakdown of the cortical cytoskeleton is thought to enhance exocytosis by allowing freer movement of vesicles below the cell surface (55–57). On the other hand, disassembly of the actin cytoskeleton prevents the structural and mechanical foundation for bulk membrane reabsorption through vesicular endocytosis (39, 40, 54). Regardless of latrunculin treatment leading to inhibition of bulk retrieval, endocytosis and exocytosis rates were found to remain normal (40). Because ATP hydrolysis is required for actin polymerization (60), ATP depletion could produce the same results. Capacitance increases recorded in this study once cells were treated with latrunculin or a combination of 2-deoxy-D-glucose and antimycin A can presumably be attributed to the same mechanism. It is also worth noting that after treatment and a resultant capacitance increase, cells still responded to stretch with additional lipid insertion. Thus it appears that although the potential of stretch increasing tensions and stimulating insertion might be buffered by previous expansion, lowered resistance to lipid insertion caused by cytoskeletal breakdown might have permitted response to lower tension stimuli.

One topic for further consideration is the interplay between plasma membrane unfolding and lipid insertion over time. Along with lipid insertion, unfolding of a convoluted cell membrane could be a crucial protection against high membrane tension. Mast cells inflated with hydrostatic pressure via micropipette quadrupled their volume without rupturing and with only slight changes in cell capacitance, indicating a substantial capacity of membrane unfolding to buffer lytic tensions (61). Viewed with an electron microscope, alveolar epithelial cells are convoluted and ruffled, suggesting a similar buffering capacity. Yet, unlike inflated mast cells, alveolar epithelial cells also insert lipids and increase their capacitance to match their size. Unfortunately, it is presently impossible to record capacitance changes in an attached cell *as it stretches* without tearing the cell membrane or losing the patch. The movement of a cell during stretch is mesoscopic relative to the microscopic size of the cell and the patch electrode, so that during stretch a cell might move tens of cell diameters away from the micropipette. Thus cells must be first stretched and then patched. In this study, the fastest patching and capacitance recordings were performed ~ 5 min after stretch, at which time, we observed, full expansion had already taken place. Using fluorescent dyes, Vlahakis and colleagues also reported that lipid trafficking had reached a steady state in alveolar epithelial cells within 60–90 s after stretch (20). Thus it appears that lipid trafficking occurs and possibly relieves tensions in stretched cells within a window of < 1 min.

To date, it is known that stretch stimulates a variety of responses in alveolar epithelial cells. Some are beneficial, so we seek to enhance them. Others are injurious, so we seek to avoid them. Less clear is how these stretch-induced responses, good or bad, are affected by the rates at which epithelial cells are stretched and the consequent fluctuations in membrane tension. Some studies addressed cell injury and plasma membrane rupture when cells are stretched a very high strain rates, and how they recover afterward (53, 62). It has also previously been reported that cells stretched at 60 cycles/min sustain greater injury than cells stretched more slowly at 15 cycles/min (63). But less is known about even lower stretch frequencies between 15 cycles/min and the 0 cycles/min of tonic stretch. Understanding the specific stimuli and responses during the tension-bearing, membrane unfolding, and lipid insertion phases of stretch could elucidate how the alveolar epithelial cell plasma membrane responds to various stretch frequencies. It is currently clear that stretch at a rate of 15 cycles/min stimulates a number of cell functions, and at least some of these functions are decreased or abolished by blocking SACs. But perhaps cells could also be stretched cyclically but so slowly that lipid insertion can take place during stretch, avoiding membrane tension increases. Although this rate may well be below what is needed to supply adequate ventilation to a mechanically ventilated patient, it may be possible to superpose low-volume, high-frequency waves with low-frequency recruitment maneuvers. Ultimately, such research might enable the identification of ventilation strategies that could target desired plasma membrane tensions, which might be associated with healthy alveolar epithelial cell responses to stretch, while reducing harmful tension levels that might overstimulate or even rupture the cell's plasma membrane.

As a first step toward such strategies, this study has found that alveolar epithelial cells undergo changes in shape and size during stretch, and, when that stretch is held tonically, cells expand their plasma membrane through lipid insertion to accommodate at least 75% of stretch-induced changes in cell surface

area within 5 min. This suggests that stretching cells over a period of 5 min or more might allow lipid insertion that could prevent high membrane tensions and possibly temper the cellular perception of stretch. However, we have also found that when released from tonic stretch, cells also reabsorb excess membrane within 5 min, meaning that tonic stretch induced relaxation is transient if stretch is not maintained. We have also determined that stretching the alveolar epithelial by stretching its adherent basement membrane to a certain percent change in surface area enlarges the entire cell surface by the same percent increase. This valuable one-to-one relationship between basal surface increase and whole cell surface area increase allows one to use traditional techniques of stretching an alveolar epithelial cell's basal surface, using a variety of custom-made or commercially available devices, and know that entire cell surface area is increasing in the same proportion. Conveniently, as a result of this finding, in making capacitance measurements, it was only necessary to take two-dimensional photographs to record change in total cell surface area. Finally, we report that lipid insertion and plasma membrane expansion appear to function at a low level linked to plasma membrane tension and are independent of actin cytoskeleton integrity, ATP availability, or calcium signaling. These findings provide an additional step toward better understanding how alveolar epithelial cells respond to stretch, and may ultimately provide insight for the development of safer, more effective ventilation strategies.

Acknowledgments: The authors thank biostatistician Dr. Warren Ewens at the University of Pennsylvania for his expert assistance with the sophisticated statistics needed to analyze and interpret the data in this study. Support for this study was provided by National Heart, Lung, and Blood Institute Grant NIH-RO1 2-HL-527204. J.L.F. was supported by a Graduate Fellowship from the Whitaker Foundation.

References

1. Margulies, S. S., J. Oswari, M. A. Matthay, and D. J. Tschumperlin. 1999. Alveolar epithelial cytoskeleton and cell vulnerability to stretch. *In* Bioengineering Conference: Proceedings of the Bioengineering Conference, 4th, 1999, Big Sky, Montana (Bed Series Vol. 42). V. K. Goel, editor. ASME Press, New York. 517–518.
2. Vlahakis, N. E., M. A. Schroeder, A. H. Limper, and R. D. Hubmayr. 1999. Stretch induces cytokine release by alveolar epithelial cells in vitro. *Am. J. Physiol.* 277:L167–L173.
3. Fisher, J. L., and S. S. Margulies. 2002. Na+-K+-ATPase activity in alveolar epithelial cells increases with cyclic stretch. *Am. J. Physiol. Lung Cell. Mol. Physiol.* 283:L737–L746.
4. Edwards, Y. S., L. M. Sutherland, J. H. Power, T. E. Nicholas, and A. W. Murray. 1999. Cyclic stretch induces both apoptosis and secretion in rat alveolar type II cells. *FEBS Lett.* 448:127–130.
5. Sanchez-Esteban, J., L. A. Cicchiello, Y. Wang, S. W. Tsai, L. K. Williams, J. S. Torday, and L. P. Rubin. 2001. Mechanical stretch promotes alveolar epithelial type II cell differentiation. *J. Appl. Physiol.* 91:589–595.
6. Pasternack, M., Jr., X. Liu, R. A. Goodman, and D. E. Rannels. 1997. Regulated stimulation of epithelial cell DNA synthesis by fibroblast-derived mediators. *Am. J. Physiol.* 272:L619–L630.
7. Cavanaugh, K. J., Jr., J. Oswari, and S. S. Margulies. 2001. Role of stretch on tight junction structure in alveolar epithelial cells. *Am. J. Respir. Cell Mol. Biol.* 25:584–591.
8. Edwards, Y. S. 2001. Stretch stimulation: its effects on alveolar type II cell function in the lung. *Comp. Biochem. Physiol. A Mol. Integr. Physiol.* 129: 245–260.
9. Liu, M., A. K. Tanswell, and M. Post. 1999. Mechanical force-induced signal transduction in lung cells. *Am. J. Physiol.* 277:L667–L683.
10. Wirtz, H. R., and L. G. Dobbs. 1990. Calcium mobilization and exocytosis after one mechanical stretch of lung epithelial cells. *Science* 250:1266–1269.
11. Tschumperlin, D. J., and S. S. Margulies. 1998. Equibiaxial deformation-induced injury of alveolar epithelial cells in vitro. *Am. J. Physiol.* 275:L1173–L1183.
12. Evans, E. 1992. Composite membranes and structured interfaces: from simple to complex designs in biology. *In* Biomembranes: Structure and Function—The State of the Art. B. P. Gaber and K. R. K. Easwaran, editors. Adenine, New York. 81–101.
13. Hamill, O. P., and B. Martinac. 2001. Molecular basis of mechanotransduction in living cells. *Physiol. Rev.* 81:685–740.
14. Raucher, D., and M. P. Sheetz. 1999. Characteristics of a membrane reservoir buffering membrane tension. *Biophys. J.* 77:1992–2002.
15. Dai, J., M. P. Sheetz, X. Wan, and C. E. Morris. 1998. Membrane tension in swelling and shrinking molluscan neurons. *J. Neurosci.* 18:6681–6692.
16. Harata, N., T. A. Ryan, S. J. Smith, J. Buchanan, and R. W. Tsien. 2001. Visualizing recycling synaptic vesicles in hippocampal neurons by FM 1–43 photoconversion. *Proc. Natl. Acad. Sci. USA* 98:12748–12753.
17. Fischer-Parton, S., R. M. Parton, P. C. Hickey, J. Dijksterhuis, H. A. Atkinson, and N. D. Read. 2000. Confocal microscopy of FM4–64 as a tool for analysing endocytosis and vesicle trafficking in living fungal hyphae. *J. Microsc.* 198:246–259.
18. Harata, N., J. L. Pyle, A. M. Aravanis, M. Mozhayeva, E. T. Kavalali, and R. W. Tsien. 2001. Limited numbers of recycling vesicles in small CNS nerve terminals: implications for neural signaling and vesicular cycling. *Trends Neurosci.* 24:637–643.
19. Hao, M., and F. R. Maxfield. 2000. Characterization of rapid membrane internalization and recycling. *J. Biol. Chem.* 275:15279–15286.
20. Vlahakis, N. E., M. A. Schroeder, R. E. Pagano, and R. D. Hubmayr. 2001. Deformation-induced lipid trafficking in alveolar epithelial cells. *Am. J. Physiol. Lung Cell. Mol. Physiol.* 280:L938–L946.
21. Pagano, R. E., and C. S. Chen. 1998. Use of BODIPY-labeled sphingolipids to study membrane traffic along the endocytic pathway. *Ann. NY Acad. Sci.* 845:152–160.
22. Pagano, R. E., R. Watanabe, C. Wheatley, and M. Dominguez. 2000. Applications of BODIPY-sphingolipid analogs to study lipid traffic and metabolism in cells. *Methods Enzymol.* 312:523–534.
23. Mayor, S., J. F. Presley, and F. R. Maxfield. 1993. Sorting of membrane components from endosomes and subsequent recycling to the cell surface occurs by a bulk flow process. *J. Cell Biol.* 121:1257–1269.
24. Hamill, O. P., A. Marty, E. Neher, B. Sakmann, and F. J. Sigworth. 1981. Improved patch-clamp techniques for high-resolution current recording from cells and cell-free membrane patches. *Pflugers Arch.* 391:85–100.
25. Gillis, K. D. 1995. Techniques for membrane capacitance measurements. *In* Single Channel Recording, 2nd ed. B. Sakmann and E. Neher, editors. Plenum Press, New York.
26. Bick, I., G. Thiel, and U. Homann. 2001. Cytochalasin D attenuates the desensitisation of pressure-stimulated vesicle fusion in guard cell protoplasts. *Eur. J. Cell Biol.* 80:521–526.
27. Henkel, A. W., H. Horstmann, and M. K. Henkel. 2001. Direct observation of membrane retrieval in chromaffin cells by capacitance measurements. *FEBS Lett.* 505:414–418.
28. Henkel, A. W., and W. Almers. 1996. Fast steps in exocytosis and endocytosis studied by capacitance measurements in endocrine cells. *Curr. Opin. Neurobiol.* 6:350–357.
29. Zupancic, G., L. Kocmur, P. Veranic, S. Grilc, M. Kordas, and R. Zorec. 1994. The separation of exocytosis from endocytosis in rat melanotroph membrane capacitance records. *J. Physiol.* 480:539–552.
30. Lewis, S. A. 2000. Everything you wanted to know about the bladder epithelium but were afraid to ask. *Am. J. Physiol. Renal Physiol.* 278:F867–F874.
31. Berrios, J. C., and R. D. Hubmayr. 2003. Deforming stress triggers endocytosis in alveolar epithelial cells. *Am. J. Respir. Crit. Care Med.* 167:A57. (Abstr.)
32. Fisher, J. L., I. Levitan, and S. S. Margulies. 2003. Changes in alveolar epithelial cell plasma membrane surface area with static stretch. 2003 Summer Bioengineering Conference of the ASME Bioengineering Division, Key Biscayne, FL.
33. Dobbs, L. G., R. Gonzalez, and M. C. Williams. 1986. An improved method for isolating type II cells in high yield and purity. *Am. Rev. Respir. Dis.* 134:141–145.
34. Kreyszig, E. 1999. Advanced Engineering Mathematics, 8th ed. Wiley, New York.
35. Morris, C. E., and U. Homann. 2001. Cell surface area regulation and membrane tension. *J. Membr. Biol.* 179:79–102.
36. Zorec, R., and M. Tester. 1993. Rapid pressure driven exocytosis-endocytosis cycle in a single plant cell: capacitance measurements in aleurone protoplasts. *FEBS Lett.* 333:283–286.
37. Wan, X., J. A. Harris, and C. E. Morris. 1995. Responses of neurons to extreme osmomechanical stress. *J. Membr. Biol.* 145:21–31.
38. Homann, U., and G. Thiel. 1999. Unitary exocytotic and endocytotic events in guard-cell protoplasts during osmotically driven volume changes. *FEBS Lett.* 460:495–499.
39. Chowdhury, H. H., M. R. Popoff, and R. Zorec. 2000. Actin cytoskeleton and exocytosis in rat melanotrophs. *Pflugers Arch.* 439:R148–149.
40. Holt, M., A. Cooke, M. M. Wu, and L. Lagnado. 2003. Bulk membrane retrieval in the synaptic terminal of retinal bipolar cells. *J. Neurosci.* 23:1329–1339.
41. Klyachko, V. A., and M. B. Jackson. 2002. Capacitance steps and fusion pores of small and large-dense-core vesicles in nerve terminals. *Nature* 418:89–92.
42. Bertorello, A. M., K. M. Ridge, A. V. Chibalin, A. I. Katz, and J. I. Sznajder. 1999. Isoproterenol increases Na^+-K^+-ATPase activity by membrane insertion of alpha-subunits in lung alveolar cells. *Am. J. Physiol.* 276:L20–L27.
43. Frick, M., S. Eschertzhuber, T. Haller, N. Mair, and P. Dietl. 2001. Secretion in alveolar type II cells at the interface of constitutive and regulated exocytosis. *Am. J. Respir. Cell Mol. Biol.* 25:306–315.
44. Voelker, D. R. 1991. Organelle biogenesis and intracellular lipid transport in eukaryotes. *Microbiol. Rev.* 55:543–560.
45. Burger, M. M., and T. Schafer. 1998. Regulation of intracellular membrane interactions: recent progress in the field of neurotransmitter release. *J. Cell. Biochem. Suppl.* 30–31:103–110.

46. Lewis, S. A., and J. L. de Moura. 1982. Incorporation of cytoplasmic vesicles into apical membrane of mammalian urinary bladder epithelium. *Nature* 297:685–688.
47. Sarikas, S. N., and F. J. Chlapowski. 1986. Effect of ATP inhibitors on the translocation of luminal membrane between cytoplasm and cell surface of transitional epithelial cells during the expansion-contraction cycle of the rat urinary bladder. *Cell Tissue Res.* 246:109–117.
48. Bacallao, R., A. Garfinkel, S. Monke, G. Zampighi, and L. J. Mandel. 1994. ATP depletion: a novel method to study junctional properties in epithelial tissues. I. Rearrangement of the actin cytoskeleton. *J. Cell Sci.* 107:3301–3313.
49. Dreyfuss, D., and G. Saumon. 1998. Ventilator-induced lung injury: lessons from experimental studies. *Am. J. Respir. Crit. Care Med.* 157:294–323.
50. Ware, L. B., and M. A. Matthay. 2000. The acute respiratory distress syndrome. *N. Engl. J. Med.* 342:1334–1349.
51. Vlahakis, N. E., and R. D. Hubmayr. 2000. Invited review: plasma membrane stress failure in alveolar epithelial cells. *J. Appl. Physiol.* 89:2490–2496.
52. Vlahakis, N. E., M. A. Schroeder, R. E. Pagano, and R. D. Hubmayr. 2002. Role of deformation-induced lipid trafficking in the prevention of plasma membrane stress failure. *Am. J. Respir. Crit. Care Med.* 166:1282–1289.
53. Thiel, G., J. U. Sutter, and U. Homann. 2000. Ca2+-sensitive and Ca2+-insensitive exocytosis in maize coleoptile protoplasts. *Pflugers Arch* 439:R152–R153.
54. Herring, T. L., C. S. Cohan, E. A. Welnhofer, L. R. Mills, and C. E. Morris. 1999. F-actin at newly invaginated membrane in neurons: implications for surface area regulation. *J. Membr. Biol.* 171:151–169.
55. Chowdhury, H. H., M. R. Popoff, and R. Zorec. 1999. Actin cytoskeleton depolymerization with clostridium spiroforme toxin enhances the secretory activity of rat melanotrophs. *J. Physiol.* 521:389–395.
56. Trifaro, J., S. D. Rose, T. Lejen, and A. Elzagallaai. 2000. Two pathways control chromaffin cell cortical F-actin dynamics during exocytosis. *Biochimie* 82:339–352.
57. Vitale, M. L., E. P. Seward, and J. M. Trifaro. 1995. Chromaffin cell cortical actin network dynamics control the size of the release-ready vesicle pool and the initial rate of exocytosis. *Neuron* 14:353–363.
58. Tsai, M. A., R. S. Frank, and R. E. Waugh. 1994. Passive mechanical behavior of human neutrophils: effect of cytochalasin B. *Biophys. J.* 66:2166–2172.
59. Hochmuth, F. M., J. Y. Shao, J. Dai, and M. P. Sheetz. 1996. Deformation and flow of membrane into tethers extracted from neuronal growth cones. *Biophys. J.* 70:358–369.
60. Alberts, B., D. Bray, J. Lewis, M. Raff, K. Roberts, and J. D. Watson. 1994. Molecular Biology of the Cell, 3rd ed. Garland Publishing, New York.
61. Solsona, C., B. Innocenti, and J. M. Fernandez. 1998. Regulation of exocytotic fusion by cell inflation. *Biophys. J.* 74:1061–1073.
62. Gajic, O., J. Lee, C. H. Doerr, J. C. Berrios, J. L. Myers, and R. D. Hubmayr. 2003. Ventilator-induced cell wounding and repair in the intact lung. *Am. J. Respir. Crit. Care Med.* 167:1057–1063.
63. Tschumperlin, D. J., J. Oswari, and S. S. Margulies. 2000. Deformation-induced injury of alveolar epithelial cells: effect of frequency, duration, and amplitude. *Am. J. Respir. Crit. Care Med.* 162:357–362.